Role of humidity in local anodic oxidation: A study of water condensation and electric field distribution

Miroslav Bartošík, David Škoda, Ondřej Tomanec, Radek Kalousek, Pavel Jánský, Jakub Zlámal, Jiří Spousta, Petr Dub, and Tomáš Šikola

Faculty of Mechanical Engineering, Institute of Physical Engineering, Brno University of Technology, Technická 2, 616 69 Brno, Czech Republic

(Received 21 October 2008; published 7 May 2009)

This paper deals with the analysis of the influence of humidity on the process of local anodic oxidation carried out by atomic force microscope (AFM) on GaAs (100) surfaces. Recent experiments have shown that the height and half width of oxide nanolines do not increase monotonously with relative humidity, but for lower relative humidities (<50%) the lines comparable in size to those prepared at 90% were obtained. However, their height and width along the lines revealed significant variations. To better understand these phenomena, the AFM force-distance spectroscopy measurements together with computer simulations of an electric-field distribution and water bridge formation between the tip and the substrate at different relative humidities were carried out. Our experiments on AFM force-distance spectroscopy have not proved an enhanced water condensation between the tip and the surface at lower humidities. However, the simulations of the electric field in the vicinity of the tip at the early stages of the oxidation process at low relative humidities showed an increase in the average intensity in the oxide layer promoting the diffusion of oxidizing species toward the substrate and, hence, the formation of oxide lines under these conditions. Finally, our simulations on water bridge variations along the tip track showed that at lower humidities there are higher relative standard deviations in the size of the water bridge while the tip is being moved along the surface. This indicates why the oxide lines showed a bigger variability in size.

DOI: 10.1103/PhysRevB.79.195406 PACS number(s): 81.16.Pr, 81.16.Nd

I. INTRODUCTION

Local formation of oxides on solid surfaces in the close vicinity of the tip of an AFM probe has become a favorite inexpensive nanotechnology method used in many laboratories worldwide. Despite the relative experimental simplicity of this technique called generally local anodic oxidation (LAO), its principles have not been understood in detail yet. The LAO is generally described by the Cabrerra-Mott[1] mechanism of oxidation adapted to the configuration with an electric field between the tip and the sample[2] providing enhanced diffusion of charged particles in the sample.[3,4] Most of the papers on LAO deals with empirical or semiempirical data related to particular materials. For instance, the influence of operational parameters on local oxidation, such as tip-sample voltage, tip writing speed, and tip load force, has been already studied using contact and noncontact modes of atomic force microscope (AFM).[5,6]

LAO depends on an ionic current between the tip and the sample surface going through a water bridge between the tip and the surface. The size and shape of this bridge depends on the amount of the water condensed both on the surface and between the tip and the surface. Generally, the amount of this water increases with humidity and, hence, it has been widely accepted that the dimensions of oxide elements produced by LAO should grow with humidity as well. This presumption has been reported by several research teams for various distinct surfaces but just few exact and detailed humidity dependences have been published yet; e.g., for *n*-Si(100),[7] *p*-Si(001),[8] and *p*-GaAs(100) substrates for relative humidity from 50–80 %.[9]

In our previous work,[10] the role of humidity in fabrication of oxide nanostructures at GaAs (100) surfaces by LAO was investigated for a wider relative humidity interval (35–90 %). Contrary to the expectations, the height and the half width of oxide nanolines grew monotonously with relative humidity just in the relative humidity interval starting from 60% up. However, for lower relative humidities (<50%), the lines were surprisingly comparable in size to those prepared at 90%. Nevertheless, unlikely to the lines at higher humidities their height and width along the lines revealed a significant variability indicating unstable conditions for the oxidation process at lower humidity.

A similar nonstandard behavior-independence of oxide height for low relative humidities under 50% and linear dependence for higher humidities has been observed by another group as well.[11] This paper deals with such a phenomenon, in a more detail, and looks for some possible key factors (e.g., water condensation, surface roughness, and electric-field distribution) responsible for this more complex behavior.

II. EXPERIMENTAL DETAILS AND PRINCIPLES

An atomic force microscope (AutoProbe CP-R, Veeco) operated in the contact mode was used both in nanolithography, microscopic, and spectroscopic experiments. The probes for nanolithography were triangular silicon cantilevers (Micromasch) with a W_2C coated tip having the average force constant 0.35 N/m and tip apex radius 35 nm, according to the producer. The real tip apex radii found by scanning electron microscope (SEM) (FEI) were in the range from 50 to 108 nm. The surface imaging and force-distance measurements were performed using rectangular phosphorus-doped silicon cantilevers (Veeco) with the average force constant

 ©2009 The American Physical Society

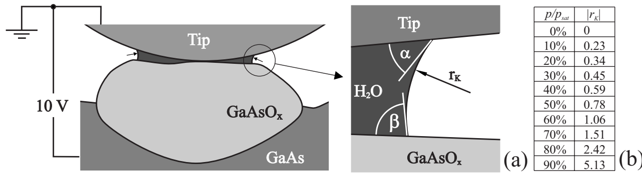

p/p_{sat}	$\lvert r_K \rvert$
0%	0
10%	0.23
20%	0.34
30%	0.45
40%	0.59
50%	0.78
60%	1.06
70%	1.51
80%	2.42
90%	5.13

FIG. 1. Local anodic oxidation by AFM. A water bridge between the tip and the surface with the (a) meniscus detail and the values of the Kelvin radius (in nm) for (b) different relative humidity.

0.9 N/m and radius below 12.5 nm (data provided by the producer).

To carry out the oxidation, a software for nanolithography (NANOLITHOGRAPHY 1.7, Veeco) was used to control the tip trajectory, tip-surface voltage, and speed and load force of the tip. The relative humidity in the working environment of AFM was controlled during the experiments by a home-built miniflow box fitted to the measuring head of the microscope. To achieve a specific relative humidity with an accuracy of 1% within the range from 20–90 %, the variable mixture of dry and H_2O-saturated nitrogen was flown through the box. The value of humidity was controlled every 10 s by a logger with an external resistive probe.

The LAO and force-distance measurements were performed on GaAs (100) substrates doped by Si (7×10^{17} atoms/cm^3) and having a specific *n*-type resistivity of 10 Ω cm. Their surface had not been treated before oxidation and spectroscopy experiments and was relatively smooth; its root-mean-square (RMS) surface roughness and average surface roughness (Ra) were 1.04 nm and 1.34 nm, respectively.

The local anodic oxidation carried out by AFM is a technique where oxides locally grow on a substrate by the application of a voltage between the conductive tip and the substrate surface acting as an anode [Fig. 1(a)]. The main process being responsible for this growth is an electric-field enhanced diffusion of oxyanions (OH^- and O^{2-}) from the condensed water to the surface. This field-induced oxidation mechanism for very thin oxide films was first described by Cabrera and Mott[1] and adapted to LAO by Stiévenard *et al.*[12] In the case of LAO on *n*-type GaAs, a depletion layer is created in the semiconductor close to its surface. Such a barrier prevents minority holes from transfer and this process stops oxidation reaction[13] unless sufficient external voltage is applied.

Except tip-sample voltage and oxidation time, the LAO process strongly depends on the amount of water adsorbed on the surface and especially on the water bridge created between the tip and the surface.[6,14] Both of these factors are influenced by relative humidity because water on hydrophilic surfaces spontaneously condenses from vapor into pores and cracks on the surface and also under the tip. At equilibrium, the water meniscus curvatures at the condensation sites are linked to the relative vapor pressure p/p_{sat} (i.e., relative humidity for water) by the Kelvin equation,[15]

$$r_K = \left(\frac{1}{r_1} + \frac{1}{r_2}\right)^{-1} = \frac{\gamma V}{RT \ln(p/p_{sat})},$$

where r_K is the Kelvin radius representing an effective radius of meniscus, r_1 and r_2 are the two principal radii of the meniscus in the horizontal and vertical cross-section planes of the meniscus, and γ and V are the surface tension and the molar volume, respectively.

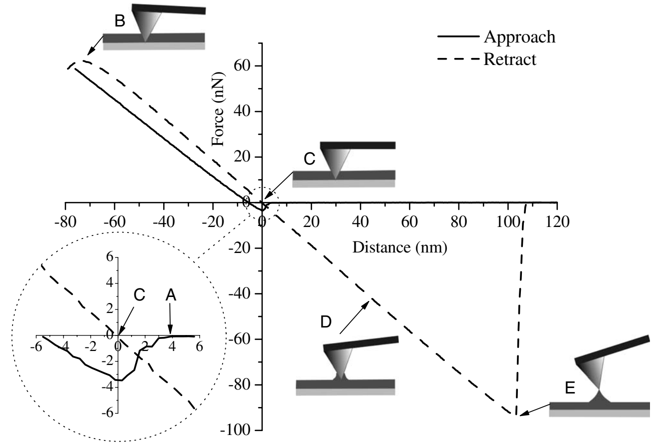

FIG. 2. Force versus distance spectroscopy (RH=91%).

The equation shows that with decreasing relative humidity the Kelvin radius becomes smaller. The dependence of the Kelvin radius on the relative humidity for water at 20 °C ($\gamma V/RT$=0.54 nm) is shown in table of Fig. 1(b).

In practice it means that at lower humidities the condensation occurs preferentially only at surface imperfections (e.g., cracks and pits) and features of higher curvatures (with the radii equal or smaller than the Kelvin radius). Concerning the condensation between the tip and the surface, the higher Kelvin radius given by higher humidities and defining the meniscus result in an increase in the neck width of the water bridge [see Fig. 1(a)]. The growth of the neck width and, hence, of the amount of condensed water results in changes in capillary forces between the tip and the surface[16] and also in the modification of an electric field in the tip-substrate area during LAO, as will be demonstrated below.

To monitor the amount of water condensed on the surface and forming the water bridge, the force-distance AFM spectroscopy was used. This method is based on measuring the dependencies of the normal force acting on the AFM tip versus the tip-sample separation during approaching/retracting the sample to/from the tip (Fig. 2). The tip first starts to experience an attractive force at the sample approach (Fig. 2: point *A*) which can be interpreted as the combination of van der Waals interaction and capillary forces related to the onset of the water bridge formation. As the sample further approaches the tip, the normal force eventually turns repulsive and reaches its maximum at the point *B* (Fig. 2: point *B*). When the sample is being retracted the force becomes zero in the point *C* and the attractive force gradually increases (Fig. 2; point *D*) to its maximum value (Fig. 2: point *E*). The distance between the tip positions corresponding to the maximum and zero capillary force (*C*-*E* distance) called the break-free length is a measure of the size of the water bridge that is formed between the tip and the sample during the contact.[17] The force-distance curves recorded in our experiments were averaged using the values from 15 approaches and retractions.

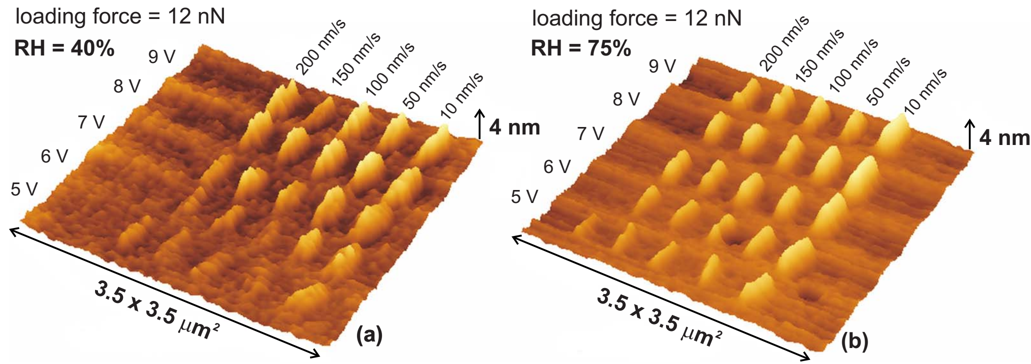

FIG. 3. (Color online) Test arrays of oxide nanolines on GaAs(100) fabricated as a function of the tip-surface voltage and tip speed at the relative humidity (a) 40% and (b) 75%. The nanolines prepared at lower humidity show up a bigger variability in height and width.

III. RESULTS AND DISCUSSION

A. Humidity effect on LAO fabricated nanostructures

Our experimental results on the role of humidity in the LAO process at GaAs(100) surfaces were presented in Ref. 9. In that work, test arrays of oxide nanolines were fabricated by LAO at various tip-sample voltages and under different relative humidities in the range 35–90 %.

The experiments showed that the lines fabricated at lower humidities (<50%) were unexpectedly comparable in size (height, depth, and half width) to those prepared at the highest once (90%); however, their height and width along the lines revealed significant variability. The size of oxide lines became stabilized at relative humidities higher than 50%. This fact is clearly observable in Fig. 3, where the AFM images of test oxide lines for relative humidities of 45% and 75%, are presented. To better understand an enhanced oxidation and size variability of lines, the force-distance spectroscopy measurements by AFM together with computer simulations of an electric-field distribution between the tip and the surface and of water condensation were performed. The results of these approaches will be discussed below.

B. Force-distance AFM spectroscopy

Figure 4 shows a plot of the maximum capillary force at five distinct surface sites of a GaAs(100) sample as a function of relative humidity. The sample had been kept for 20 min under specific humidity atmosphere and then the spectroscopy measurements were carried out at these selected sites inside the area $200 \times 200\ \text{nm}^2$. In the figure inset, there is a plot of the force values averaged over the test sites and provided with the calculated standard deviations. The corresponding break-free length determined by the conversion of the average capillary force shown in the inset of Fig. 4 is presented in Fig. 5.

A maximum possible effort was made to keep the identical test sites for measurements at different relative humidities. Despite that fact the obtained values are loaded with big errors, nevertheless, they give us useful information on the curve development. As mentioned above, the break-free length is a measure of the size of the water bridge between the tip and the sample.

The break-free length (and force values) is low for relative humidities around 20% and 60%. When the relative humidity exceeds 60%, it starts quickly to grow. It represents the growth of the width of the water bridge which has also been confirmed by our simulations (see below). There is a local maximum of the capillary force and break-free length around the relative humidity 40%. However, the standard deviations of the break-free length are big and so the local maximum might not be a true one. Further, the values of the Kelvin radius for lower humidities are smaller than 1 nm (see Sec. II and table in Fig. 1) and the RMS surface roughness is about 1 nm, which means that the size of surface corrugations and imperfections is even bigger. It means that there is no coincidence of the Kelvin radius at this humidity with the size of these features which should have resulted in an enhanced water condensation and so in a more efficient oxidation process induced by the tip. Hence, the force-distance spectroscopy has not confirmed this effect and, therefore, other processes should be responsible for the development of bigger oxide lines at lower humidities.

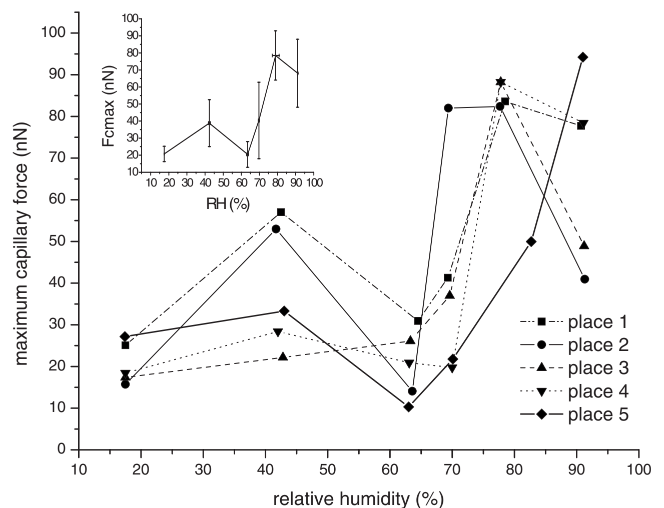

FIG. 4. Maximum capillary force between the tip and the surface during the sample retraction as a function of relative water humidity. In the inset, the force values averaged over the test sites and provided with the corresponding standard deviations.

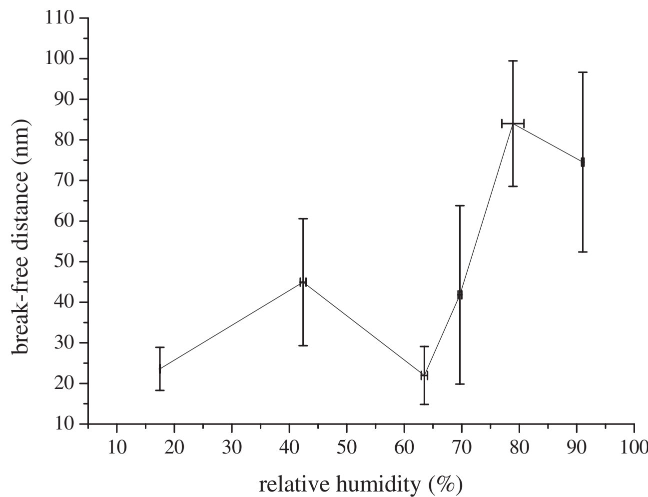

FIG. 5. The break-free length as a function of relative humidity corresponding to the capillary force experiments in Fig. 4

C. Simulation of water condensation under the tip moving over a surface

To better understand the formation of the water bridge between the tip and the surface under different humidities, the computer simulation was carried out using a code written in the VISUAL BASIC. The code simulates water bridge profiles in four cross-sectional vertical planes of the bridge above the specific site. Each plane is rotated from the neighboring one by 45° (Fig. 6). The boundary conditions of the meniscus were defined by water contact angles [Fig. 1(a)] at the sample surface (β=76° determined in a separate experiment for the GaAs substrate covered with a native oxide by optical microscopy) and at the silicon tip surface (α=38° measured on a phosphorus-doped silicon substrate by optical microscopy), as well as by the Kelvin radius calculated from the Kelvin equation for a given humidity [Fig. 1(b)]. The tip apex radius was approximated in the simulations by a sphere with a radius of 65 nm (determined by the SEM measurements of the real tips).

To find how the size of the water bridge changes from one to another surface site (and thus to explain the variations in line height and width along the oxide lines), the tip was moved in simulations over the surface in the x direction along four different lines and floated at the distance 0.3 nm from the nearest point of the surface (constant height mode). The simulation utilized experimental-surface-morphology data provided by AFM on the GaAs (100) surface over an area of 200×200 nm^2. In the LAO experiment, the writing speed was just 10 nm/s. Hence, the tip passed particular sites for the relatively long time which justifies the application of the equilibrium Kelvin radius theory in our simulations.

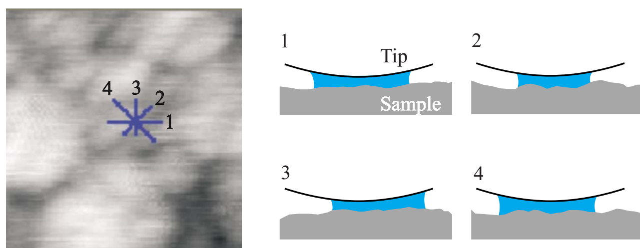

FIG. 6. (Color online) Simulation of water meniscus in four different planes at one surface site.

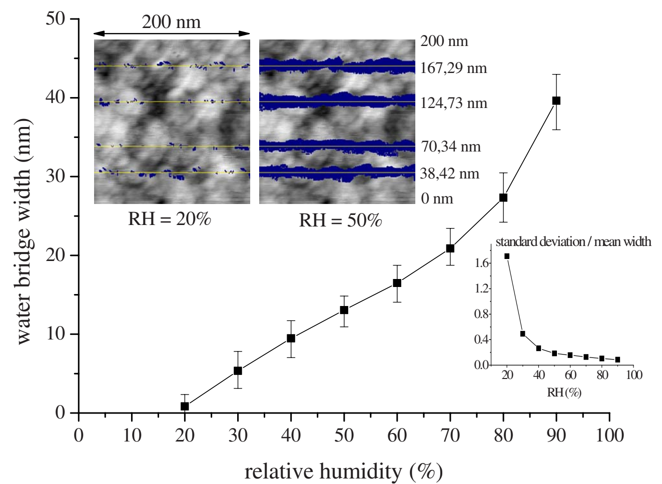

FIG. 7. (Color online) The width of the water bridge between the tip and the surface as a function of relative humidity; ratios of the standard deviation to the mean width (bottom right inset); development of an area given by the projection of a simulated water bridge into the surface during the tip movement from the left to the right for two different humidities (top left inset).

In each test point, the diameters of the water bridge at the contact point with the substrate surface were calculated in all the four cross-sectional planes. The track made of the water surface areas defined by these diameters (projection of the water bridges) at different test points along the scanned lines is drawn in blue in Fig. 7 (top left inset). Further, in this figure the average track width (i.e., the water bridge diameter in the y direction over the whole track) along with its standard deviation as a function of relative humidity is plotted as well. As expected, the size of the water bridge and so the track width increases monotonously with humidity because the Kelvin radius grows with this parameter as well – the growing Kelvin radius increases the probability that the envelope of the bridge represented by the meniscus will form the required contact angle to the local surface features at higher radial distances from the center of the water bridge than in case of low humidities (small Kelvin radii). As the standard deviation grows with the humidity much more slowly the relative deviation of the track width expressed by the ratio of the standard deviation to the mean width goes up with decreasing humidity (Fig. 7, bottom right inset). This explains bigger variations in cross-sectional dimensions (height and width) of oxide lines being observed mostly at lower values of relative humidity.

Supposing the main source of oxyanions is water, the water bridge size is important in the determination of the width of oxide lines. In accordance with that a reduction in lateral dimensions of dots fabricated by LAO with a decrease in the water bridge width controlled by the tip-surface distance was observed.[12] On the other hand, the width of simulated water bridges in Fig. 7 does not correspond to that of the real oxide lines, which were several times broader.[9] However, the width

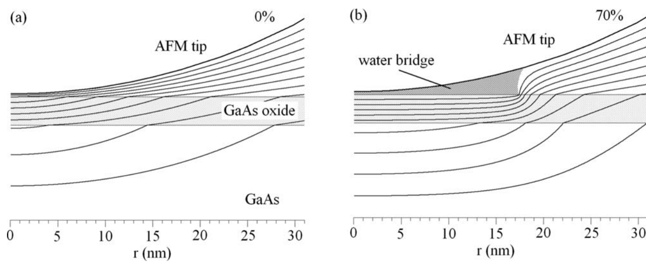

FIG. 8. The equipotential lines in the vicinity of an AFM tip and the model sample consisting of a native GaAs oxide layer and GaAs substrate. Without the water bridge at the (a) relative humidity 0% and with the water bridge at the (b) relative humidity 70%. The thickness of the tip-sample gap, GaAs oxide layer, and GaAs substrate chosen for the simulations was 0.3 nm, 2.5 nm, and 10 nm, respectively.

of oxide lines is an interplay of more factors and besides the size of the reservoir of oxyions (water bridge) it also depends on an electric-field distribution between the tip and the surface. This will be discussed in the next section.

D. Simulation of the electric field in the tip vicinity

To imagine the forces governing the diffusion of ions in the early stage of the LAO process, the simulation of an electric field in the nearest neighborhood of the AFM tip was performed using the EOD (electron optical design) code[18] based on the finite element method (FEM). Particularly, the influence of the water bridge (the size of which depends on relative humidity) on the electric-field distribution between the tip and the surface was studied. The distribution of equipotential lines between the tip and the sample surface shows that the occurrence of the water bridge results in "pushing" the equipotential lines out of the tip-sample space into the native oxide layer of the GaAs sample beneath, as demonstrated in Fig. 8. This is a direct consequence of significant differences in relative permittivities of water ($\varepsilon_r=81$), GaAs oxide ($\varepsilon_r=3.5$), and GaAs ($\varepsilon_r=13.9$). In this sense the water meniscus can be considered as a lens concentrating the electric field into the layer of GaAs oxide. This enhances the electric field in the whole oxide layer and, hence, a diffusion of ions through it.

Figure 9 shows a radial distribution (taken from the tip apex center) of the magnitude of electric-field intensity in the GaAs oxide layer in a depth of 0.25 nm under its surface for different humidities. Under dry conditions (relative humidity 0%), the equipotential lines are not pushed out of the tip-sample space into the oxide layer and the electric field in the oxide layer is smaller and falls down from the center according to a Gaussian-type function. Under the total wet conditions (relative humidity 100%) the surface is fully covered with water; therefore no significant "pushing" of the lines into the oxide layer occurs and thus only a slight increase in the electric-field intensity is observed here. The field is almost constant over relatively large radial distances from the tip (falling down just due to the finite curvature of the tip). The electric-field profiles for humidities between these two extremes (dry and fully wet) differ substantially from the

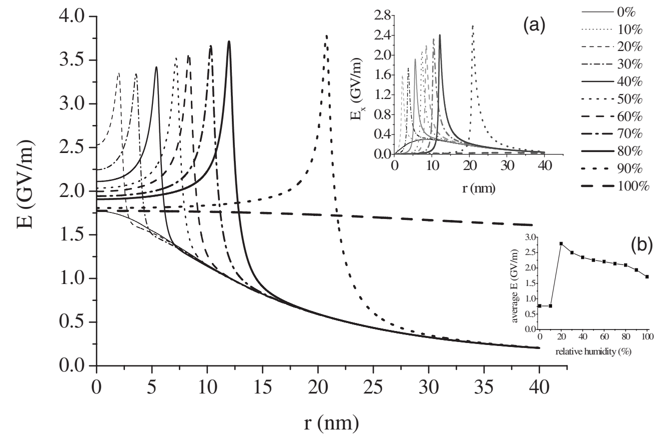

FIG. 9. The radial profiles of the magnitude of electric intensity in the GaAs oxide layer 0.25 nm deep below its surface for different relative humidities; the radial $\bar{x}$ component of electric-field intensity [inset (a)]; the average value of the magnitude of electric intensity in the oxide layer under the water bridge [inset (b)].

previous ones. In the central part of the investigated tip area, the electric-field intensity is the highest for the lowest humidities and, generally, its radial profiles have a peaklike character at radial distances corresponding to the edge of the water bridge. As a consequence of it the average value of the magnitude of electric-field intensity in the oxide layer under the water bridge is higher for lower relative humidities (Fig. 9 inset). This effect contributes at lower humidities to the formation of the oxide structures of a similar size such as in the case of higher humidities, as demonstrated in Fig. 3. However, to quantify it, additional simulations have to be done yet.

Further, pushing the equipotential lines into the substrate by the water bridge causes a rise of the radial component of the electric-field intensity at radial distances closer to the edge of the water bridge (Fig. 9). This effect can contribute to an additional lateral enlargement of the oxide area far beyond the space defined by the water meniscus.

IV. CONCLUSION

To better understand an enhanced oxidation and size variability of oxide lines at lower humidities reported in our previous paper, the force-distance spectroscopy measurements by AFM together with computer simulations of an electric-field distribution between the tip and substrate and of water condensation, respectively, were performed. Our experiments on AFM force-distance spectroscopy have not proved an enhanced water condensation between the tip and the surface at lower humidities. Hence, more intensive growth of oxide lines under low humidities reported in our previous work cannot be explained by this effect. The AFM-force-distance spectroscopy confirmed enhanced water condensation only at higher humidities which was in line with our simulations.

On the other hand, the simulations of the electric field in the vicinity of the tip at the early stages of the oxidation process showed an increase in the average intensity in the

oxide layer for lower humidities. This contributes to an enhanced diffusion of reactive ions and thus certainly to the more intense development of oxide lines under these conditions. The enhanced radial component of the electric intensity at radial distances closer to the edge of the water bridge at all relative humidities could be one of the reasons for an additional lateral enlargement of the oxide area beyond the space defined by the water bridge

The profound size variations in oxide lines observed at low humidities indicate variability in the oxidation process when the tip is moved over the surface under these conditions. This occurs as a result of the less probable water condensation between the tip and the surface at low humidities resulting from the smaller Kelvin radius of the meniscus Our simulations showing variations in the water bridge size along the tip track at different relative humidities support this idea.

ACKNOWLEDGMENTS

This work was supported by the research programs of the Ministry of Education of the Czech Republic (Projects No. MSM0021630508 and No. LC04060), GAAV (Projects No. IAA1010413 and No. KAN400100701), and GACR (Project No. FON/06/E001).

[1] N. Cabrera and N. F. Mott, Rep. Prog. Phys. **12**, 163 (1949).

[2] D. Stiévenard, P. A. Fontaine, and E. Dubois, Appl. Phys. Lett. **70**, 3272 (1997).

[3] H. Kuramochi, F. Peréz-Murano, J. A. Dagata, and H. Yokoyama, Nanotechnology **15**, 297 (2004).

[4] S. F. Lyuksyutov, P. B. Paramonov, I. Dolog, and R. M. Kalich, Nanotechnology **14**, 716 (2003).

[5] P. A. Fontaine, E. Dubois, and D. Stiévenard, J. Appl. Phys. **84**, 1776 (1998).

[6] J. Cervenka, R. Kalousek, M. Bartosik, D. Skoda, O. Tomanec, and T. Sikola, Appl. Surf. Sci. **253**, 2373 (2006).

[7] P. Avouris, T. Hertel, and R. Martel, Appl. Phys. Lett. **71**, 285 (1997).

[8] H. Kuramochi, K. Ando, and H. Yokoyama, Surf. Sci. **542**, 56 (2003).

[9] S.-R. Jian, T.-H. Fang, and D.-S. Chuu, J. Phys. D **38**, 2424 (2005).

[10] M. Bartosik, D. Skoda, O. Tomanec, R. Kalousek, P. Jansky, J. Zlamal, J. Spousta, and T. Sikola, J. Phys.: Conf. Ser. **61**, 75 (2007).

[11] C. Albonetti, J. Martinez, Nuria S. Losilla, Pierpaolo Greco, Massimiliano Cavallini, Francesco Borgatti, Monica Montecchi, Luca Pasquali, Ricardo Garcia, and Fabio Biscarini, Nanotechnology **19**, 435303 (2008).

[12] D. Stiévenard, P. A. Fontaine, and E. Dubois, Appl. Phys. Lett. **70**, 3272 (1997).

[13] S. K. Ghandhi, *VLSI Fabrication Principle*, 2nd ed. (Wiley, New York, 1994).

[14] R. Garcia, M. Calleja, and H. Rohrer, J. Appl. Phys. **86**, 1898 (1999).

[15] J. Israelachvili, *Intermolecular and Surface Forces*, 2nd ed. (Academic Press, San Diego, 1992).

[16] T. Stifter, O. Marti, and B. Bhushan, Phys. Rev. B **62**, 13667 (2000).

[17] M. Binggeli and C. M. Mate, Appl. Phys. Lett. **65**, 415 (1994).

[18] B. Lencova and J. Zlamal, Microsc. Microanal. **13**, 2 (2007).